Additive Manufacturing Letters 4 (2023) 100114

Contents lists available at ScienceDirect

Additive Manufacturing Letters

journal homepage: www.elsevier.com/locate/addlet

Thermal properties of copper nanoparticles at different sintering stages governed by nanoscale heat transfer

Jihoon Jeong [a,1], Yaguo Wang [a,b,*]

[a] J. Walker Department of Mechanical Engineering, The University of Texas at Austin, Austin, TX 78712, United States
[b] Texas Materials Institute (TMI), The University of Texas at Austin, Austin, TX 78712, United States

ARTICLE INFO

Keyword:
Cu nanoparticles
Microscale selective laser sintering
Thermoreflectance
Thermal conductivity
Nanoscale heat transfer

ABSTRACT

Utilizing metal nanoparticles (NPs) in Additive Manufacturing (AM) enables fabricating parts with sub-micrometer resolution. The thermal properties of metal NPs are drastically different from their bulk and micron-size counterparts due to nanoscale thermal transport effects, e.g. ballistic phonon/electron transport instead of diffusive transport described by Fourier's Law. Rough estimation of metal NPs' thermal properties with bulk values will inevitably cause large errors for AM applications, because thermal properties evolve along with the sintering process. In this study, thermal properties of 100 nm Cu NPs are examined at different sintering stages. Effective density is measured between 3500 and 5300 kg/m^3 at a sintering temperature range of 100 and 400 °C, and the sintering of Cu NPs is determined to be around 300 °C using Thermogravimetry analysis (TGA) with Differential Scanning Calorimeter (DSC). A picosecond Transient Thermoreflectance (ps-TTR) technique is employed to measure the effective thermal conductivity of Cu NPs, which jumps from 18.5 ± 0.8 W/m•K to 26.8 ± 2.1 W/m·K onset of sintering around 300 °C. These values are less than 1/10 of the bulk value (398 W/m·K). The effective thermal conductivity is almost independent on porosity except in the temperature range close to 300 °C, which comes from two factors related with nanoscale thermal transport: (i) ballistic electron transport is important in particles with size comparable with electron mean free path; (ii) effective thermal conductivity is dominated by interface scattering on particles surfaces. Our results provide insights about the importance on accurate characterization of thermal properties in metal nanoparticles due to the nanoscale phenomena.

1. Introduction

Additive manufacturing (AM) is an advanced manufacturing technique that adds material in patterned layers to build a desired shape part [1,2] and can reduce process complexity and cost [3,4]. Among a variety of AM processes, selective laser melting (SLM) and selective laser sintering (SLS) are capable to fabricate objects out of a wide range of materials including metals, ceramics, and polymers [1,2]. However, current commercially available microscale AM processes are constrained in a few ways: (a) many techniques can work only with polymers, via two-photon lithography and interface lithography; (b) very challenging to produce specific three-dimensional (3-D) structures, such as electrohydrodynamic jet printing and direct ink writing; (c) too slow to be used in large quantity manufacturing processes, such as electrochemical deposition. These limitations make them incompatible with many applications, especially electronics packaging applications or electrical circuits for electronic devices [5]. Recently, a new AM technique called microscale selective laser sintering (μ-SLS) has been developed [6,7], that is able to produce 3-D metallic parts with sub-5 μm feature size. This μ-SLS requires usage of ink-form metal particles with nanometer-scale sizes to achieve dense parts with desirable mechanical properties. The μ-SLS process include three key steps: (1) nanoparticle bed formation, (2) sintering of particles, and (3) high precision sample transfer and alignment [7].

For all the SLS/SLM processes, knowing the thermal properties before and during the sintering is critical to predict/determine the optimum sintering parameters for producing desirable final products. So far, thermal properties of metal particles used in SLS/SLM are usually estimated based on bulk counterparts [8,9]. Determination of thermal properties experimentally is challenging due to lack of proper techniques, which result in very few studies reported in literature. Wei et al. [10] applied the hot-wire method to measure the effective thermal conductivity of five different metal powders with a nominal diameter about 35 μm and concluded that, at the unsintered conditions, the effective thermal conductivity is only less than 1% of the solid bulk materials. Ebrahmimi et al. [11] measured the thermal conductivity of 32 μm (diameter) cop-

* Corresponding author.
E-mail address: yaguo.wang@austin.utexas.edu (Y. Wang).
[1] Present address: Department of Mechanical Engineering, Northwestern University, Evanston, IL 60208, USA

https://doi.org/10.1016/j.addlet.2022.100114
Received 27 October 2022; Received in revised form 3 December 2022; Accepted 4 December 2022

per particles using a parallel-plate set up with thermocouples and reported a value of 1.5 W/m·K for un-sintered particles and 30 W/m·K for sintered particles. (As a reference, the thermal conductivity of bulk copper is about 398 W/m·K).

Difference of the thermal conductivity values between bulk and nanoparticles (NPs) is expected to be even more dramatic. Lin et al. [12] reported an effective thermal conductivity value of 2.5 W/m·K for a copper packed bed with particle size of 50 nm and 4 W/m·K with a particle size of 500 nm using a hot-wire method. Y. Son et al. [13] reported thermal conductivity of ink-form Ag NPs with 3 ~ 6 nm using a laser flash method and obtained a value of 0.37 W/m·K, 3 orders smaller than that of bulk silver (429 W/m·K). Even though only few, results from literature reveal that the effective thermal conductivity of metal particles highly depends on the particle size and form (e.g. powder bed or ink). Ink form is preferred for sintering of metal NPs to avoid the agglomeration effect, which becomes even more severe with NPs.

All these previous measurements focus on unsintered particles, even though one or two studies also measured the sintered parts. During the sintering process, effective thermal conductivity may change continuously along with neck-formation but the history of thermal conductivity evolution during sintering is largely unknown. In this study, the effective thermal properties of ink-form Cu NPs at different sintering stages will be characterized with a non-destructive picosecond transient thermoreflectance (ps-TTR) technique to improve understanding of heat transfer among Cu NPs for μ-SLS. The thermal behavior of Cu NPs will be investigated to identify the sintering temperature and actual heat capacity will also be discussed. Density of unsintered and sintered Cu NPs are also measured. It is found that the effective thermal conductivity of Cu NPs behaves very different from that in micro particles, due to the nanoscale thermal transport effect.

2. Material and methods

Cu NPs ink was prepared (100 nm; Applied Nanotechnology; IJ-70) and spin-coated on a glass substrate (Laurel, WS-650Mz-23NPPB) as shown in Fig. 1(a). The coated glass with Cu NPs was dried at 100 ˚C for 30 min to remove the organic solvent residue. Then, the heat treatment was conducted for the coated glass with Cu NPs at different temperatures to achieve thermal sintering at different stages. A tube furnace with an Ar atmosphere was employed to sinter Cu NPs to avoid oxidation. Cu NPs were heat treated at each target temperature for 2 h.

Scanning Electron Microscopy (SEM) is employed for microstructure analysis, and the results are shown in Fig. 2. As the sintering temperature increases, the Cu NPs are getting connected and bonded, and the well-connected features among the Cu NPs are observed in the sample sintered at 400 ˚C. It is well known that bulk Cu is melted at 1085 ˚C, but the NPs can be melted at a much lower temperature.

For density measurement, weight was measured by subtracting mass before and after Cu NPs coated on the glass substrate. Volume was obtained via the following approach: with the image of the Cu NPs coated on the glass, the area was firstly measured, and the thicknesses at 5 different locations across the whole sample were measured using an optical profilometer (Keyence; VK-X1100). The average value of the scanned thickness was used to calculate the volume with the measured area, and the density was estimated as: $\rho_{measured}$ = mass/volume. Porosity (ε) was approximated from the measured density ($\rho_{measured}$) and bulk Cu density (ρ_{bulk}): ε=1-($\rho_{measured}/\rho_{bulk}$). When the porosity ($\varepsilon$) is 0, a sample is fully densified.

Thermogravimetry analysis (TGA) with Differential Scanning Calorimeter (DSC) was conducted to observe the thermal behavior of Cu NPs to determine the sintering temperature of the Cu NPs (Mettler; model TGA/DSC1). The temperature was ramped to 500 ˚C with 10 K/min and two different atmospheres (air and N_2) were tested.

For thermal conductivity measurement, a 50-nm Au layer was deposited on a glass substrate as a metal transducer. Then Cu NPs ink (> 1 μm) was spin-coated on the Au layer so that the pump and the probe can be delivered onto the Au layer through the transparent glass for obtaining a temperature change on the Au surface as shown in Fig. 1(c). The Cu NPs layer of > 1 μm is necessary for thermal conductivity measurement to assume Cu NPs as a semi-infinite substrate so that all heat absorbed by the Au layer is transferred and dissipated within the Cu NPs. The rest of the preparation processes are the same as the density measurement sample preparation including drying and heat treatment at target temperatures. The picosecond transient thermoreflectance (ps-TTR) technique was employed to measure the thermal conductivity of Cu NPs [14]. The ps-TTR system includes a picosecond pulse laser as the heating source (Coherent Talisker Ultra 532–8, 1064 nm, and repetition rate of 200 kHz) and a continuous wave (CW) probe laser (Coherent Verdi 532 nm) (see Supplemental Material for a schematic diagram of ps-TTR setup). The pump and probe spot sizes ($1/e^2$ diameter) are 120 μm and 10 μm, respectively. The reflected probe signal is monitored by an Avalanche Photodiode (APD) detector (Hamamatsu C5658, 1 GHz bandwidth) with an oscilloscope (TDS 744A, 2Gbs sampling rate). Because pump spot size is much larger than the sample thickness and probe spot size , a 1D heat conduction model in a multilayer sample (glass/Au/Cu NPs) is assumed. Volumetric heat capacity (J/m^3) is used for thermal conductivity measurement while bulk heat capacity and effective density are used.

3. Results

Density measurements are conducted under different sintering temperatures, as shown in Fig. 3(a). The density values are measured between 3500 and 5300 kg/m^3 from 100 to 400 ˚C (bulk value of 8960 kg/m^3). The density value starts to increase from a temperature of 250 ˚C and is saturated at a temperature of 350 ˚C, which indicates that the Cu NPs begin to be sintered. Fig. 3(b) plots porosity estimated using density measurement results, which shows an opposite trend with temperature because when the density increases, porosity decreases accordingly. These results suggest that the density/porosity values can change dramatically during the sintering process and should be determined *in-situ* for various purposes, such as for accurate prediction of final product properties with simulations and determination of *in-situ* thermal conductivity change.

TGA/DSC measurement can provide actual sintering temperature information since Cu NPs are expected to have much lower sintering temperatures than micron-size or even bigger Cu particles due to size effect. It is well-known that NPs have lower sintering temperatures due to their

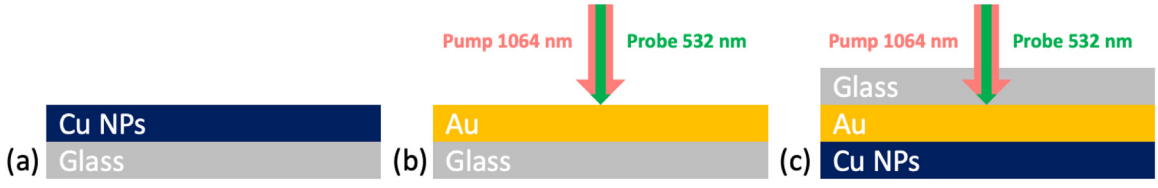

Fig. 1. Sample preparation for (a) density measurement of Cu NPs and (b) thermal conductivity and interfacial resistance measurement of Au and glass, $R_{Au/glass}$ and κ_{glass}, and (c) thermal conductivity and interafcial resistanc of Cu NPs, $R_{Au/CuNPs}$ and κ_{CuNPs}.

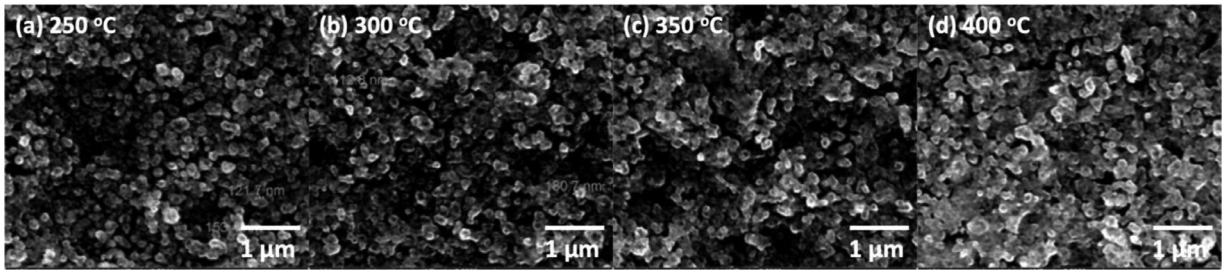

Fig. 2. Microstructure of sintered Cu NPs at different temperatures of (a) 250 ˚C, (b) 300 ˚C, (c) 350 ˚C, and (d) 400 ˚C captured by SEM.

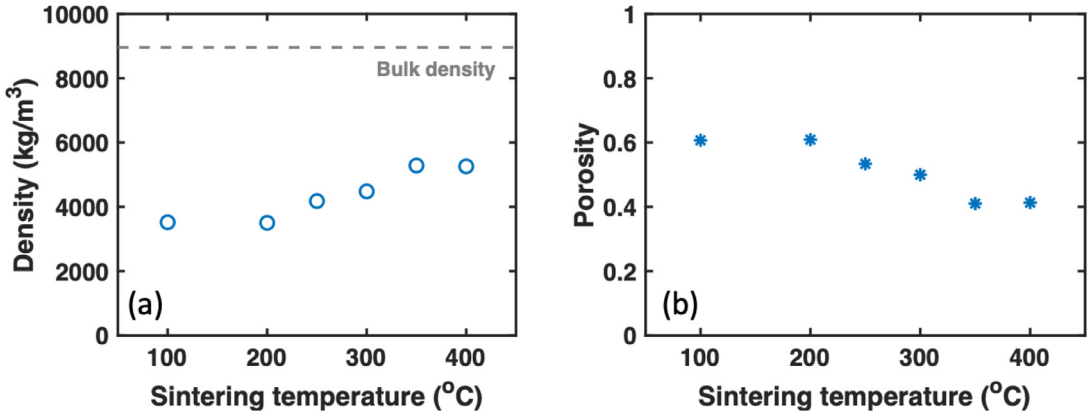

Fig. 3. (a) Density measurement results and (b) estimated porosity under different sintering temperatures.

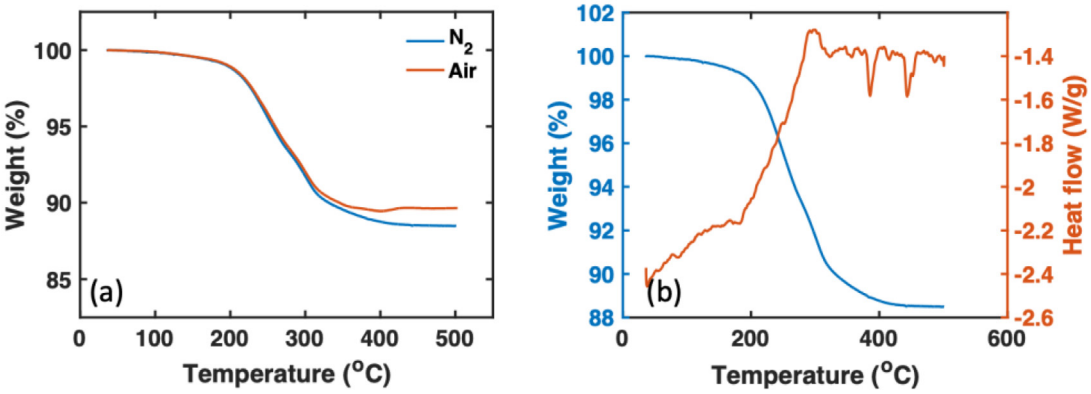

Fig. 4. Thermal behavior observation using TGA/DSC: (a) TGA results at N_2 and air atmospheres and (b) TGA/DSC results at N_2 atmosphere.

high activity [16]. Fig. 4(a) shows that a significant mass change in both atmospheres appears up to 300 ˚C, which indicates the removal of organics or carbon coatings included in the ink. After 300 ˚C, the mass change starts to slow down and eventually saturates, also the trends in air/N_2 start to diverge. Under air, above 300 ˚C, the mass percentage is always higher than that under N_2, which indicates the occurrence of oxidation of Cu NPs in air. From the DSC measurement, the sintering behavior is further confirmed by the heat flow involved during heating the Cu, as shown in Fig. 4(b). The heat flow increases rapidly above 200 ˚C, and then stabilizes around 300 ˚C, which also signals the onset of sintering. Combining the SEM images of microstructure change with the TGA/DSC results, thermal sintering of Cu NPs starts at about 300 ˚C.

Heat capacity of Cu NPs can also be estimated from the DSC measurement result. As shown in Fig. 4(b), that heat flow becomes stable at 1.4 W/g from 300 ˚C. According to the TGA result, no significant mass change happens after 300 ˚C so most of the heat is spent to heat up the Cu NPs for phase change (melting/partial melting), and this is the point from which heat capacity can be calculated. Since the temperature ramp rate is 10 K/min, the heat capacity is estimated as 1.4 W/g × 10 K/min = 233.3 J/kg•K, which is about 60% of bulk heat capacity (385 J/kg•K). This 60% of the bulk heat capacity value is consistent with the density measurement result, and these results indicate that the Cu NPs samples are a mixture of Cu NPs and ambient gas with 6:4 ratio. In literature, heat capacity in NPs sometimes is larger than bulk [15] and, the bulk value of heat capacity is used, and effective density is used for micron-size particles [11]. It is important to point out that the effective heat capacity and effective density could not be used simultaneously in thermal conductivity analysis, which will double count the lower mass effect in NPs and cause unreasonable thermal conductivity values.

In the multilayer sample geometry shown in Fig. 1(c), two interfaces are involved: Au/Glass interface and Au/Cu NPs interface. The thermal interfacial resistance at Au/Glass interface ($R_{Au/glass}$) is predetermined using ps-TTR with Au coated on a glass microscope slide as shown in Fig. 1(b) (without any Cu NPs), along with the thermal conductivity of glass (κ_{glass}). The extracted values are $R_{Au/glass}$ = 25.9 m^2•K/GW

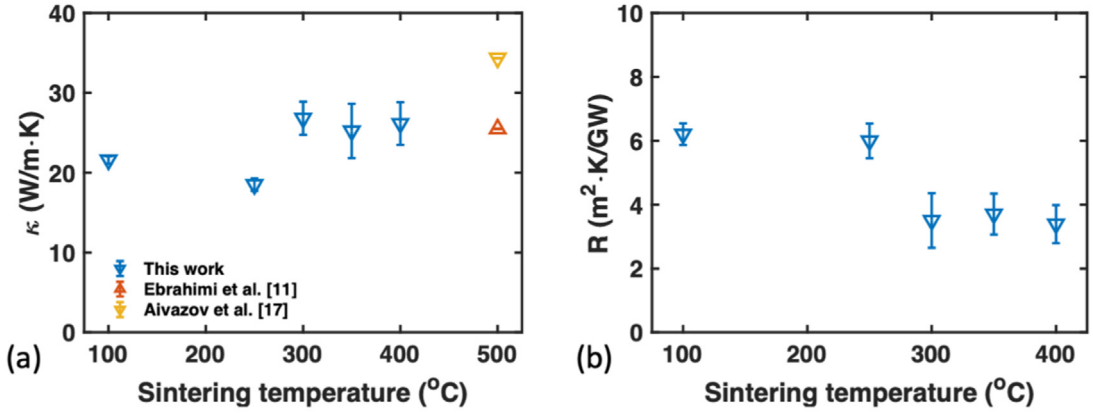

Fig. 5. Results of (a) thermal conductivity of Cu NPs compared with reported values [11,17] (micron size particles), and (b) interfacial thermal resistance between Au and Cu NPs measured by ps-TTR.

and κ_{glass} = 1.58 W/m•K, which are consistent with the reported values [14,18]. These values are used as input parameters in the 1D heat conduction model to fit the experimental data to determine the thermal conductivity of Cu NPs (κ_{CuNPs}) and interfacial thermal resistance value between Au and Cu NPs ($R_{Au/CuNPs}$). Since the Au layer is always prepared with e-beam deposition under the same conditions, the values of $R_{Au/glass}$ and κ_{glass} are not expected to change within the temperature range of the sintering experiment (250 ~ 400 °C).

Measured thermal conductivity values of Cu NPs under different sintering temperatures are plotted in Fig. 5(a). Below 250 °C, the κ_{CuNPs} is around 18.5 ± 0.8 W/m•K. Around 300 °C, a big jump occurs, above which the κ_{CuNPs} increases to around 26.8 ± 2.1 W/m•K. It is interesting to observe that the fluctuation of κ_{CuNPs} above 300 °C is below the detection limit of our system. There is clear evidence that effective thermal conductivity (κ_{CuNPs}) increases with the onset of sintering, mainly due to the formation of necks among NPs that overcomes the thermal resistance caused by the air gap among particles and the particle/particles interfaces. Even though at higher temperatures, the microstructure with SEM image shows more necking among particles and we may expect further improvement of thermal conductivity, this increase could be small compared to the effect from the initial necking around 300 °C. Even though the effective thermal conductivity increases by about 35% with sintering onset, this value is only about 5% of the bulk thermal conductivity of Cu, 398 W/m•K. It is surprisingly small when considering the 60% effective density after sintering, which indicates that the air gaps and interfaces among NPs are very effective as thermal barriers. These results suggest that the traditional approach to evaluate the effective thermal conductivity with effective density is far away from the real scenario, and would cause a large discrepancy between the design and actual manufacturing products for the AM process. Fig. 5(b) shows that the $R_{Au/CuNPs}$ decreases from 6.2 ± 0.3 m²•K/GW to below 3.4 ± 0.6 m²•K/GW. This trend is as expected because the melted NPs at the Au/NPs interface increases the contact area and reduce the thermal resistance.

4. Discussion

There have been many studies to investigate a relationship between porosity and effective thermal conductivity of sintered metal particles. In Fig. 6, our measured values of κ_{CuNPs} are plotted together with results reported in literature (both experimental results [11,19,20] and simulations [17,21,22]) as a function of porosity. By comparing the data, there are two main differences: (1) at similar porosity, our measured κ_{CuNPs} are much lower than the literature results. (2) before and after the onset of sintering, our measured κ_{CuNPs} do not show obvious dependence on porosity, except for the jump at around 300 °C. It is worth to point out all these literature results are about the micron-size Cu particles, while ours are for the Cu NPs. It is not a surprise to observe much lower

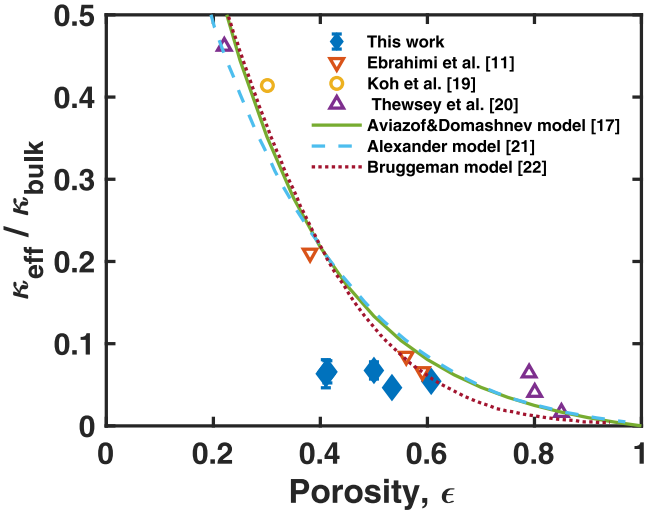

Fig. 6. Normalized thermal conductivities of sintered Cu particles as a function of the porosity compared with the references for both experimental results [11,19,20] and simulations [17,21,22].

thermal effective thermal conductivity in Cu NPs. However, independence of porosity is somewhat counter intuitive. The two discrepancies described above can be understood from the perspective of different heat conduction mechanisms at nano- and micro- scale. Nanoscale heat transfer has been a very active field for three decades [23–25]. At large scale, heat carriers (phonons and/or electrons) in solids propagate diffusively and the thermal conductivity can be extracted via Fourier's law. When the characteristic length reduces to an extent that is comparable with the electron/phonon mean free path (the average path electron/phonon travels without any scattering event), the possibility that electron/phonons can travel across the whole sample without any scattering (Ballistic Heat Transfer) increases. This ballistic behavior of thermal transport has two consequences: (i) size-dependent thermal conductivity; and (ii) violation of Fourier's law. In metals, the main heat carriers are electrons. For Cu, the electron mean free path is about 40 nm [26]. In the micron-size Cu particles, electrons propagate diffusively and the size effect is not important. The thermal conductivity of each individual Cu particle should be close to that of bulk values. The overall effective thermal conductivity is still governed by the mass volume of particles themselves, which explains the strong dependence on porosity. Our Cu NPs have nominal diameter about 100 nm, comparable with the electron mean free path and hence size effect becomes important. Within individual Cu NP, most electrons travel ballistically and the thermal conductivity is governed by the boundary scattering at NP surface, no longer

the mass volume of particles. As a result, the overall effective thermal conductivities are determined by the surface area of Cu NPs, which can be related with surface-volume ratios. Surface area per volume (SA/V) can be calculated for spherical particles using a formula of $3/r_p$ [27]. For comparing Cu NPs of 100 nm diameter with Cu micron-sized particles of 35 μm, SA/V for each particle is 6×10^6 and 1.7×10^5, respectively. Cu NPs have more than 35 times the surface area for the same volume, which explains the much lower effective thermal conductivity of Cu NPs, as well as the independence on porosity. When the sintering starts to occur around 300 ˚C, surface area of NPs can experience a large decrease due to necking and hence the surface scatterings are reduced, which result in a thermal conductivity jump. At higher temperature, the neck can grow thicker but the overall surface area is not going to change significantly, so does the effective thermal conductivity. There are also experiment and simulation studies for nanoparticle composites that suggest the thermal conductivity of NP composites can be lower than the alloy value due to a high interface density [28,29], which is a consistent interpretation with our observation. Note that Grose et al. [30] recently reported the particle thermal model to calculate the thermal conductivity of Cu NPs as a function of the density of the NPs. According to the reported value, the predicted thermal conductivity of the NPs at the effective density of 5300 kg/m^3 is 22.7 ± 6.3 W/m·K, which is consistent with our measured thermal conductivity value of 26.2 ± 2.7 W/m·K.

5. Conclusion

The thermal properties of Cu NPs are characterized at different sintering stages, including effective density, sintering temperature, and effective thermal conductivity. Effective density is measured between 3500 and 5300 kg/m^3 at a sintering temperature range of 100 and 400 ˚C, and the sintering of Cu NPs starts above 300 ˚C, which is very low compared to the bulk melting temperature of 1085 ˚C. A picosecond Transient Thermoreflectance (ps-TTR) technique is employed to measure the effective thermal conductivity of Cu NPs, which jumps from 18.5 ± 0.8 W/m•K to 26.8 ± 2.1 W/m·K onset of sintering around 300 ˚C. These values are less than 1/10 of the bulk value (398 W/m·K). The effective thermal conductivity is almost independent on porosity except in the temperature range close to 300 ˚C. This can be understood from two aspects: (1) non-diffusive (ballistic) heat transfer occurs in NPs with size comparable with electron mean free path; and (2) an increase in the surface area producing large boundary scatterings that hinder heat transfer across NPs.

Declaration of Competing Interest

The authors declare that they have no known competing financial interests or personal relationships that could have appeared to influence the work reported in this paper.

Data availability

Data will be made available on request.

Acknowledgment

This work was supported by National Science Foundation under Grant CBET-1934357.

Supplementary materials

Supplementary material associated with this article can be found, in the online version, at doi:10.1016/j.addlet.2022.100114.

References

[1] J.P. Kruth, M.C. Leu, T. Nakagawa, Progress in additive manufacturing and rapid prototyping, CIRP Ann. 47 (2) (1998) 525–540.
[2] I. Gibson, D.W. Rosen, B. Stucker, M. Khorasani, D. Rosen, B. Stucker, M. Khorasani, Additive Manufacturing tech- Nologies, 17, Springer, 2021.
[3] I. Theodorakos, F. Zacharatos, R. Geremia, D. Karnakis, I. Zergioti, Selective laser sintering of Ag nanoparticles ink for applications in flexible electronics, Appl. Surf. Sci. 336 (2015) 157–162.
[4] X. Yu, B.K. Mahajan, W. Shou, H. Pan, Materials, mechanics, and patterning techniques for elastomer-based stretchable conductors, Micromachines 8 (1) (2016) 7 (Basel).
[5] N. Roy, W. Jou, H. Feng, J. Jeong, Y. Wang, M. Cullinan, Laser sintering of copper nanoparticles: a simplified model for fluence estimation and validation, in: Proceedings of the International Manufacturing Science and Engineering Conference, 50732, American Society of Mechanical Engineers, 2017 V002T01A032.
[6] N.K. Roy, O.G. Dibua, W. Jou, F. He, J. Jeong, Y. Wang, M.A. Cullinan, A comprehensive study of the sintering of copper nanoparticles using femtosecond, nanosecond, and continuous wave lasers, J. Micro Nano Manuf. 6 (1) (2018).
[7] N.K. Roy, D. Behera, O.G. Dibua, C.S. Foong, M.A. Cullinan, A novel microscale selective laser sintering (μ-sls) process for the fabrication of microelectronic parts, Microsyst. Nanoeng. 5 (1) (2019) 1–14.
[8] C.W. Cheng, J. Chen, Femtosecond laser sintering of copper nanoparticles, Appl. Phys. A 122 (4) (2016) 1–8.
[9] Y. Ren, J. Chen, Y. Zhang, Optical properties and thermal response of copper films induced by ultrashort-pulsed lasers, J. Appl. Phys. 110 (11) (2011) 113102.
[10] L.C. Wei, L.E. Ehrlich, M.J. Powell-Palm, C. Montgomery, J. Beuth, J.A. Malen, Thermal conductivity of metal powders for powder bed additive manufacturing, Addit. Manuf. 21 (2018) 201–208.
[11] N.D. Ebrahimi, Y.S. Ju, Thermal conductivity of sintered copper samples prepared using 3d printing-compatible polymer composite filaments, Addit. Manuf. 24 (2018) 479–485.
[12] Z.Z. Lin, C.L. Huang, W.K. Zhen, Z. Huang, Enhanced thermal conductivity of metallic nanoparticle packed bed by sintering treatment, Appl. Therm. Eng. 119 (2017) 425–429.
[13] Y. Son, J. Yeo, C.W. Ha, J. Lee, S. Hong, K.H. Nam, D.Y. Yang, S.H. Ko, Application of the specific thermal properties of Ag nanoparticles to high-resolution metal patterning, Thermochim. Acta 542 (2012) 52–56.
[14] J. Jeong, X. Meng, A.K. Rockwell, S.R. Bank, W.P. Hsieh, J.F. Lin, Y. Wang, Picosecond transient thermoreflectance for thermal conductivity characterization, Nanoscale Microscale Thermophys. Eng. 23 (3) (2019) 211–221.
[15] B.. Wang, L.. Zhou, X.F. Peng, Surface and size effects on the specific heat capacity of nanoparticles, Int. J. Thermophys. 27 (1) (2006) 139–151.
[16] F. Gao, Z. Gu, in: Melting Temperature of Metallic Nanoparticles, in: Handbook of Nanoparticles, Springer, 2016, pp. 661–690.
[17] M. Aivazov, I. Domashnev, Influence of porosity on the conductivity of hot-pressed titanium-nitride specimens, Sov. Powder Metall. Met. Ceram. 7 (9) (1968) 708–710.
[18] J. Yang, E. Ziade, A.J. Schmidt, Uncertainty analysis of thermoreflectance measurements, Rev. Sci. Instrum. 87 (1) (2016) 014901.
[19] J. Koh, A. Fortini, Prediction of thermal conductivity and electrical resistivity of porous metallic materials, Int. J. Heat Mass Transf. 16 (11) (1973) 2013–2022.
[20] D. Thewsey, Y. Zhao, Thermal conductivity of porous copper manufactured by the lost carbonate sintering process, Phys. Status Solidi 205 (5) (2008) 1126–1131.
[21] E.G. Alexander, Structure-Property Relationships in Heat Pipe Wicking Materials JR, North Carolina State University, 1972.
[22] D. Bruggeman, The calculation of various physical constants of heterogeneous substances. i. the dielectric constants and conductivities of mixtures composed of isotropic substances, Ann. Phys. 416 (1935) 636–791 (N Y).
[23] D.G. Cahill, W.K. Ford, K.E. Goodson, G.D. Mahan, A. Majumdar, H.J. Maris, R. Merlin, S.R. Phillpot, Nanoscale thermal transport, J. Appl. Phys. 93 (2) (2003) 793–818.
[24] D.G. Cahill, P.V. Braun, G. Chen, D.R. Clarke, S. Fan, K.E. Goodson, P. Keblinski, W.P. King, G.D. Mahan, A. Majumdar, et al., Nanoscale thermal transport. II. 2003–2012, Appl. Phys. Rev. 1 (1) (2014) 011305.
[25] H. Zhan, Y. Nie, Y. Chen, J.M. Bell, Y. Gu, Thermal transport in 3d nanostructures, Adv. Funct. Mater. 30 (8) (2020) 1903841.
[26] A. Mallikarjunan, S. Sharma, S. Murarka, Resistivity of copper films at thicknesses near the mean free path of electrons in copper minimization of the diffuse scattering in copper, Electrochem. Solid State Lett. 3 (9) (2000) 437.
[27] Y. Ghasemi, M. Emborg, A. Cwirzen, Estimation of specific surface area of particles based on size distribution curve, Mag. Concr. Res. 70 (10) (2018) 533–540.
[28] M.S. Jeng, R. Yang, D. Song, G. Chen, Modeling the thermal conductivity and phonon transport in nanoparticle composites using Monte Carlo simulation, J. Heat Transf. 130 (4) (2008).
[29] C. Bera, N. Mingo, S. Volz, Marked effects of alloying on the thermal conductivity of nanoporous materials, Phys. Rev. Lett. 104 (11) (2010) 115502.
[30] J. Grose, O.G. Dibua, D. Behera, C.S. Foong, M. Cullinan, Simulation and property characterization of nanoparticle thermal conductivity for a microscale selective laser sintering system, J. Heat Transf. (2022).